ORIGINAL ARTICLE

A Novel Porcine Model of CLN2 Batten Disease that Recapitulates Patient Phenotypes

Vicki J. Swier[1] · Katherine A. White[1] · Tyler B. Johnson[1] · Jessica C. Sieren[2,3] · Hans J. Johnson[6] ·
Kevin Knoernschild[2,3] · Xiaojun Wang[4] · Frank A. Rohret[4] · Christopher S. Rogers[4] · David A. Pearce[1,5] ·
Jon J. Brudvig[1,5] · Jill M. Weimer[1,5]

Abstract

CLN2 Batten disease is a lysosomal disorder in which pathogenic variants in *CLN2* lead to reduced activity in the enzyme tripeptidyl peptidase 1. The disease typically manifests around 2 to 4 years of age with developmental delay, ataxia, seizures, inability to speak and walk, and fatality between 6 and 12 years of age. Multiple *Cln2* mouse models exist to better understand the etiology of the disease; however, these models are unable to adequately recapitulate the disease due to differences in anatomy and physiology, limiting their utility for therapeutic testing. Here, we describe a new $CLN2^{R208X/R208X}$ porcine model of CLN2 disease. We present comprehensive characterization showing behavioral, pathological, and visual phenotypes that recapitulate those seen in CLN2 patients. $CLN2^{R208X/R208X}$ miniswine present with gait abnormalities at 6 months of age, ERG waveform declines at 6–9 months, vision loss at 11 months, cognitive declines at 12 months, seizures by 15 months, and early death at 18 months due to failure to thrive. $CLN2^{R208X/R208X}$ miniswine also showed classic storage material accumulation and glial activation in the brain at 6 months, and cortical atrophy at 12 months. Thus, the $CLN2^{R208X/R208X}$ miniswine model is a valuable resource for biomarker discovery and therapeutic development in CLN2 disease.

Keywords CLN2 Batten disease · Miniswine · Cortical atrophy · Electroretinogram a- and b-waves · Gait · Seizures

Introduction

Batten disease (neuronal ceroid lipofuscinoses) is a family of rare autosomal recessive disorders with more than 10 variants and is collectively the most common neurodegenerative pediatric disorder [1]. Cellular dysfunction occurs when storage material accumulates in the lysosomes of cells,

resulting in a cascade of events leading to gliosis and neurodegeneration concentrated in select regions of the brain and spinal cord [2]. One of the variants of Batten disease, ceroid lipofuscinosis neuronal 2 (CLN2), is caused by pathogenic variations in the lysosomal enzyme tripeptidyl peptidase 1 (TPP1), resulting in reduced or absent enzyme activity and lysosomal dysfunction. CLN2 onset typically occurs at 2 to 4 years of age and quickly progresses to include vision loss, motor and cognitive decline, ataxia, and seizures [3]. Advances in therapeutic development have led to one approved therapy, an enzyme replacement therapy called cerliponase alfa (Brineura), for CLN2 disease. Cerliponase alfa slows functional decline but does not halt brain graymatter loss and thus leaves patients with substantial unmet needs. No cure exists and, if untreated, patients generally succumb to the disease between 6 and 12 years of age. Of the 155 known pathogenic variants in CLN2 [4], c.509-1G > C and p.Arg208X (nonsense mutation) are the most frequently occurring in the patient population accounting for 57% of all identified *TPP1* mutant alleles [5].

Our team previously generated a $Cln2^{R207X/R207X}$ mouse model with the equivalent human p.Arg208x pathogenic

✉ Jill M. Weimer
Jill.Weimer@sanfordhealth.org

[1] Pediatrics and Rare Diseases Group, Sanford Research, Sioux Falls, SD, USA

[2] Department of Radiology, University of Iowa, Iowa City, IA, USA

[3] Department of Biomedical Engineering, University of Iowa, Iowa City, IA, USA

[4] Precigen Exemplar, Coralville, IA, USA

[5] Department of Pediatrics, Sanford School of Medicine, University of South Dakota, Sioux Falls, SD, USA

[6] Department of Electrical and Computer Engineering, University of Iowa, Iowa City, IA, USA

variant [6]. This model, as well as previously developed *Cln2*^{−/−} mouse models [7], recapitulate many of the behavioral and pathological phenotypes of the disease [1, 3, 8]. However, large animal models often better recapitulate critical aspects of human disease and response to therapies, making them extremely useful for preclinical toxicology and efficacy studies [9–11]. For example, a naturally occurring *TPP1*^{−/−} dog model has shown excellent utility in preclinical studies; however, it has limitations in that it does not recapitulate a common pathogenic variant [9–13]. Other naturally occurring animal models of NCL, such as the CLN5 and CLN6 ovine model, as well as the transgenic CLN1 ovine model (with a common occurring human pathogenic variation) have recapitulated patient phenotypes and elucidated many of the mechanisms of the disease, demonstrating the potential of transgenic large animal models for Batten disease research and therapeutics [14–18].

Miniswine are another attractive large animal preclinical model, given their long history of targeted genetic modifications and improved somatic cell nuclear transfer techniques that have enhanced this species' use for biomedical research [19]. Swine are anatomically similar to humans, especially in regards to a gyrencephalic brain, and have a similar lifespan and size [20]. Of all commonly used model organisms, miniswine also offer the closest approximation of human body surface area, enabling more accurate calculation and utilization of human equivalent doses for preclinical studies [21]. Many swine models of neurological diseases have already been characterized and used for a variety of purposes including neurological disease modeling [22–25], clinical imaging using human-grade equipment [26–30], and biomarker development and preclinical testing [31, 32].

Here, we have developed a novel miniswine model of CLN2 disease harboring a R208X mutation that demonstrates significant utility as a model, recapitulating many of the phenotypes seen in patients. Combined with the aforementioned advantages of miniswine as a preclinical model, *CLN2*^{R208X/R208X} miniswine will have excellent utility for investigations into the basic biology of CLN2 disease, the identification of biochemical and imaging biomarkers for early diagnosis and disease progression, and the testing of therapeutics.

Results

Generation of CLN2^{R208X/R208X} Miniswine

Recombinant AAV-mediated gene targeting was used to introduce the CLN2 mutation in Yucatan miniswine fetal fibroblasts as previously described [22, 23, 29, 33]. Briefly, male Yucatan fetal fibroblasts were infected with rAAV

carrying a targeting construct designed to introduce the human CLN2 mutation (R208X) into the porcine ortholog (Supplemental Fig. 1). The resulting *CLN2*^{+/R208X} fibroblasts were used as nuclear donors for somatic cell nuclear transfer, and reconstructed embryos were transferred to recipient pigs. CLN2-targeted miniswine were born following a 114-day gestation, and heterozygote progenitor miniswine were then bred to generate the *CLN2*^{R208X/R208X} homozygotes used in this study.

A study design schematic is presented in Fig. 1A, with 44 animals (wild-type: 8 females/10 males; *CLN2*^{R208X/R208X}: 12 females/14 males) monitored every 3 months from approximately 3 to 19 months of age for qualitative monitoring/survival assessment, retinal function via electroretinography (ERG), motor function via temporal-spatial gait analysis, and cognitive function via a simple t-maze. Histological correlates of lysosomal storage material accumulation, neuroinflammation, and neurodegeneration were analyzed at 6, 12, and 18 months of age. Additionally, a separate cohort of 18 female animals were monitored throughout the period for qualitative assessment and neuroimaging tests at 12 and 18 months of age (wild-type: 6 females; *CLN2*^{R208X/R208X}: 12 females). A single sex was used for the neuroimaging studies due to the cost-limiting nature of imaging an appropriately-powered large animal study, and females were chosen due to reports of female patients with Batten disease experiencing a late onset, but more severe disease course [34, 35].

CLN2^{R208X/R208X} Miniswine Show Overt Vision Loss, Gait Abnormalities, and Early Death

Neurological function was monitored over the 3- to 19-month period. *CLN2*^{R208X/R208X} animals presented with obvious vision loss at approximately 15 months of age (females) and 16.5 months of age (males). Vision deficits manifested as animals walking into walls/gates and failing to track an experimenter's hand (Fig. 1B). Poor balance and overt mobility declines started to arise on average at 16 months of age (females) and 17.5 months of age (males) (Fig. 1C). Severe hindlimb ataxia/hypermetria manifested on average at 19 months of age in male *CLN2*^{R208X/R208X} animals but the median age of onset for loss of hindlimb use was undefined in female *CLN2*^{R208X/R208X} as only 12% of females showed the phenotype (Fig. 1D). Additionally, one *CLN2*^{R208X/R208X} male presented with multiple spontaneous tonic seizures at 15 months of age, and two *CLN2*^{R208X/R208X} females presented with seizures at 16 months of age (Fig. 1E). Though significant differences exist between *CLN2*^{R208X/R208X} animals and their sex-matched wild-type counterparts, there are no significant differences between male and female *CLN2*^{R208X/R208X} animals at the age of onset of these phenotypes.
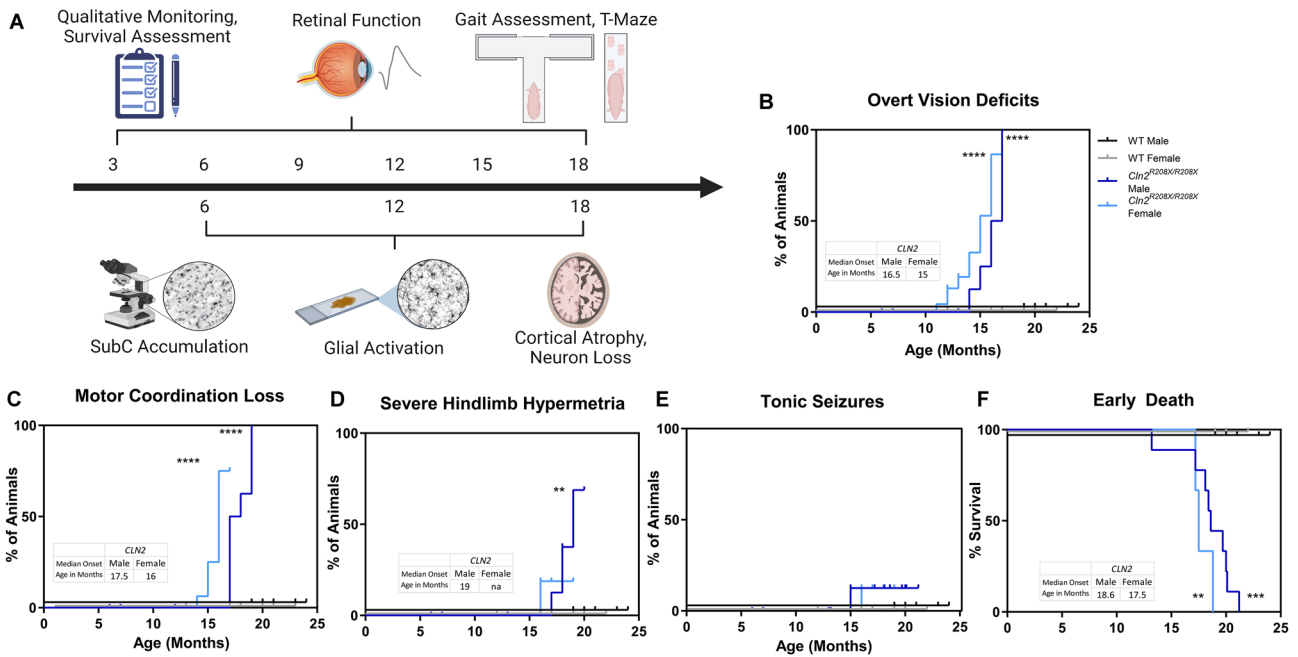
Fig. 1 $CLN2^{R208X/R208X}$ swine show overt vision loss, motor impairments, and premature death. **A** Animals were monitored for phenotypic presentation and behavioral assays at 3, 6, 9, 12, 15, and 18 months of age, and were assessed for histology at 6, 12, and 18 months of age. **B** Percent of animals showing obvious vision issues, as deemed by animals showing vision loss behaviors such as running into walls or not tracking a hand that is waved in front of their eyes. **C** Percent of animals showing poor walking and balance, as deemed by animals splaying out their limbs, limping, etc. **D** Percent of animals showing severe hindlimb ataxia, manifested as complete loss of hindlimb use. **E** Percent of animals presenting spontaneous tonic seizures. **F** Survival curve through 25 months of age. Animal numbers in Supplementary Table 1. Log-rank Mantel-Cox test with Bonferroni correction, asterisks represent comparisons between sex-matched WT controls $*p < 0.05$, $**p < 0.01$, $***p < 0.001$, $****p < 0.0001$

Abnormal feeding behavior indicated by a loss of appetite and abnormal social behavior (noted as unusually quiet animals that were unresponsive to other miniswine and animal care staff) were recorded after onset of clinical symptoms at approximately 14 months of age. Compared to wild-type, body condition score and weight began to decline as $CLN2^{R208X/R208X}$ animals reached the 15-month time point and continued to decline up to 18–19 months of age. These animals rapidly lost coordination of their limbs, were unable to reach food and water unassisted, and were determined to have reached a humane endpoint. $CLN2^{R208X/R208X}$ animals were euthanized as early as 10 months of age, but on average, animals reached humane endpoints at 17.5 months of age (females) and at 18.6 months of age (males) (Fig. 1F). Additionally, as these animals aged, liver enzyme function declined as noted by significantly increased levels of aspartate aminotransferase (AST) in serum of 18-month-old animals (Supplemental Fig. 2A, B). Creatine kinase levels were also elevated in five of the eight $CLN2^{R208X/R208X}$ males examined, and the male with multiple seizures had a creatine kinase value of 12,941 U/L at the time of euthanasia (normal values for swine: 129–1409 U/L) (Supplemental Fig. 2C, D).

CLN2^{R208X/R208X} Miniswine Show Cognitive and Motor Impairment by 6 to 12 Months of Age

Animals were assessed for cognitive and motor deficits every three months from 3 to 18 months of age. A simple t-maze was used as a measurement of memory and learning, in which animals were given two days to learn and recall the correct location of a food reward (acquisition days 1 and 2) and 2 days to learn and recall the location of a food reward that was moved to a new location (reversal days 1 and 2). While both wild-type and $CLN2^{R208X/R208X}$ animals performed similarly in the acquisition portions of the experiment (Fig. 2A, C, E; acquisition days 1 and 2), both male and female $CLN2^{R208X/R208X}$ animals showed deficits in reversal by 12 months of age, as demonstrated by fewer correct responses in finding food in the new arm (Fig. 2B, D, F, reversal days 1 and 2). Learning deficits on reversal day 1 persisted in $CLN2^{R208X/R208X}$ males at 15 months, but statistical support was lost in females at that time point, though the animals did continue to make fewer correct responses. At 18 months of age, $CLN2^{R208X/R208X}$ females did not make any correct choices, and males averaged less than 2 correct choices (Fig. 2D–F). On reversal day 2, $CLN2^{R208X/R208X}$ learning deficits were observed at 18 months in females and
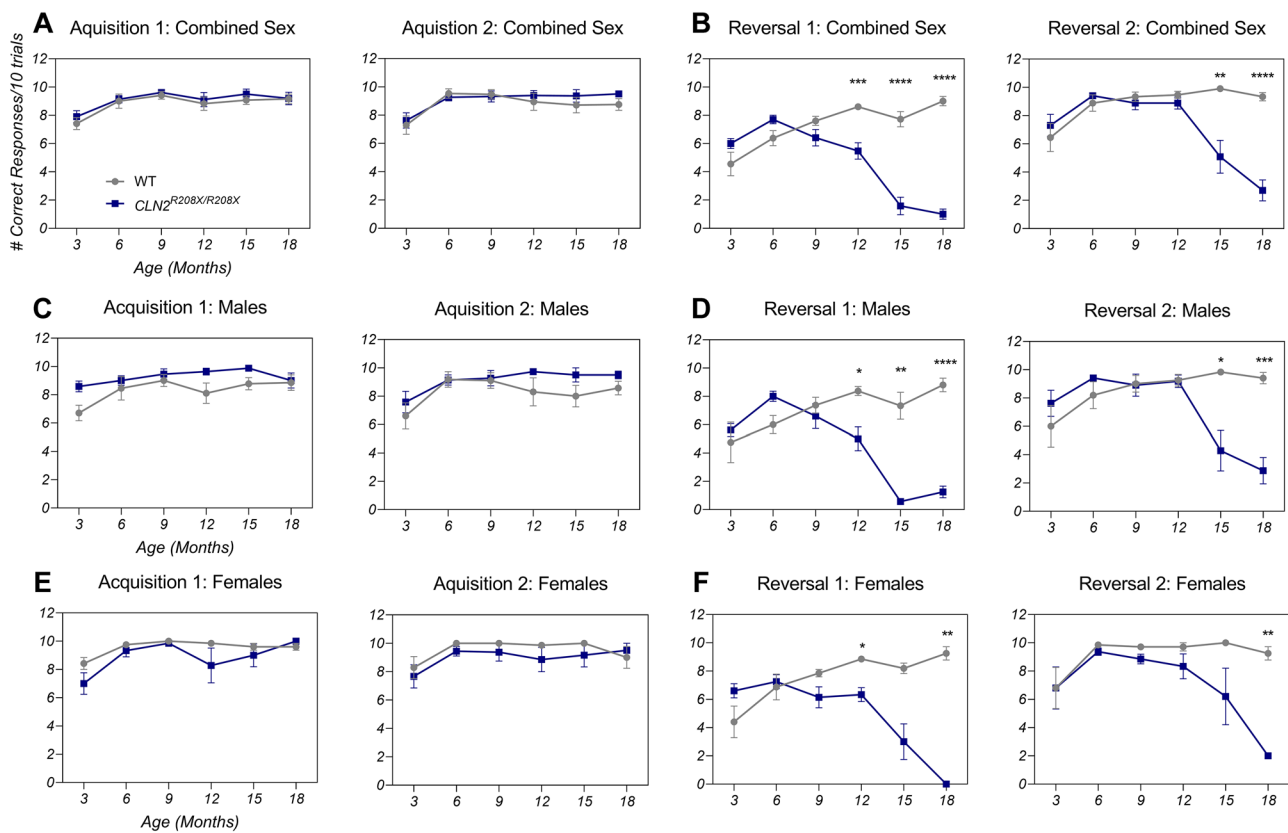
Fig. 2 $CLN2^{R208X/R208X}$ animals show deficits in a simple T-maze by 12 months of age. **A**, **B** Simple t-maze results for combined sexes, including acquisition tests and reversal tests. **C**, **D** Simple t-maze results for male animals and **E**, **F** female animals, showing that both sexes of $CLN2^{R208X/R208X}$ animals show similar deficits. Animal numbers in Supplementary Table 1. Mean ± SEM, Mixed-model ANOVA with Sidak's multiple comparisons. $*p < 0.05$, $**p < 0.01$, $***p < 0.001$, $****p < 0.0001$

both 15 and 18 months in males (Fig. 2B, D, F, reversal day 2).

Gait was assessed with a Zeno Electronic Walkway sensor mat (ZenoMetrics Peekskill, NY), where 153 variables were extracted from front and hind feet independently and analyzed using a principal component analysis (PCA). Using this technique, $CLN2^{R208X/R208X}$ animals showed a significantly altered front foot gait beginning at 6 months of age and continuing through 18 months of age, with more prominent abnormalities in male animals (Fig. 3A–C). The front foot first principal component (PC1) was composed of 28 parameters associated with 'foot strike' (foot placement and pressure upon the mat), 'temporal' metrics (time/speed variables), and 'spatial' metrics (length and width measurements). Within these categories, PC1 was defined by 4 variables and their variances: Stance COP (center of pressure of a single footfall), foot area, stride velocity, and stride/step length; indicating that only a few variables are necessary to track disease progression (Fig. 3D). The parameters that contributed most to these differences included foot area, in which $CLN2^{R208X/R208X}$ male front foot strike is significantly

smaller by 9 months of age (Fig. 3E); stride velocity, as shown by slower stride velocity at 6, 9, and 18 months (Fig. 3F); and stride length as shown by shorter strides and steps at 6, 9, 12, and 18 months (Fig. 3G). Hind foot analysis showed similar, but less severe, differences in wild-type and $CLN2^{R208X/R208X}$ gait beginning at 6 months of age and continuing through 18 months of age, which was detected earlier in male animals (Supplemental Fig. 3A–C). The hind foot PC1 was composed of 25 variables, with the greatest weighted variables including foot area, stance COP, and stride/step length (Supplemental Fig. 3D). The change in the WT gait score from 12 to 15 months of age may be reflective of the reduction in the number of animals at 12 M (7F; 9 M) compared to 15 M (5F; 8 M).

Lastly, locomotion and general activity was monitored using a FitBark Activity Monitor as previously described [36]. While there were some significant differences between genotypes (distance traveled in males-Supplemental Fig. 4A; percent of day resting in males and females-Supplemental Fig. 4B; and sleep quality in males and females-Supplemental Fig. 4D), these differences were transient and not sustained as the animals aged.
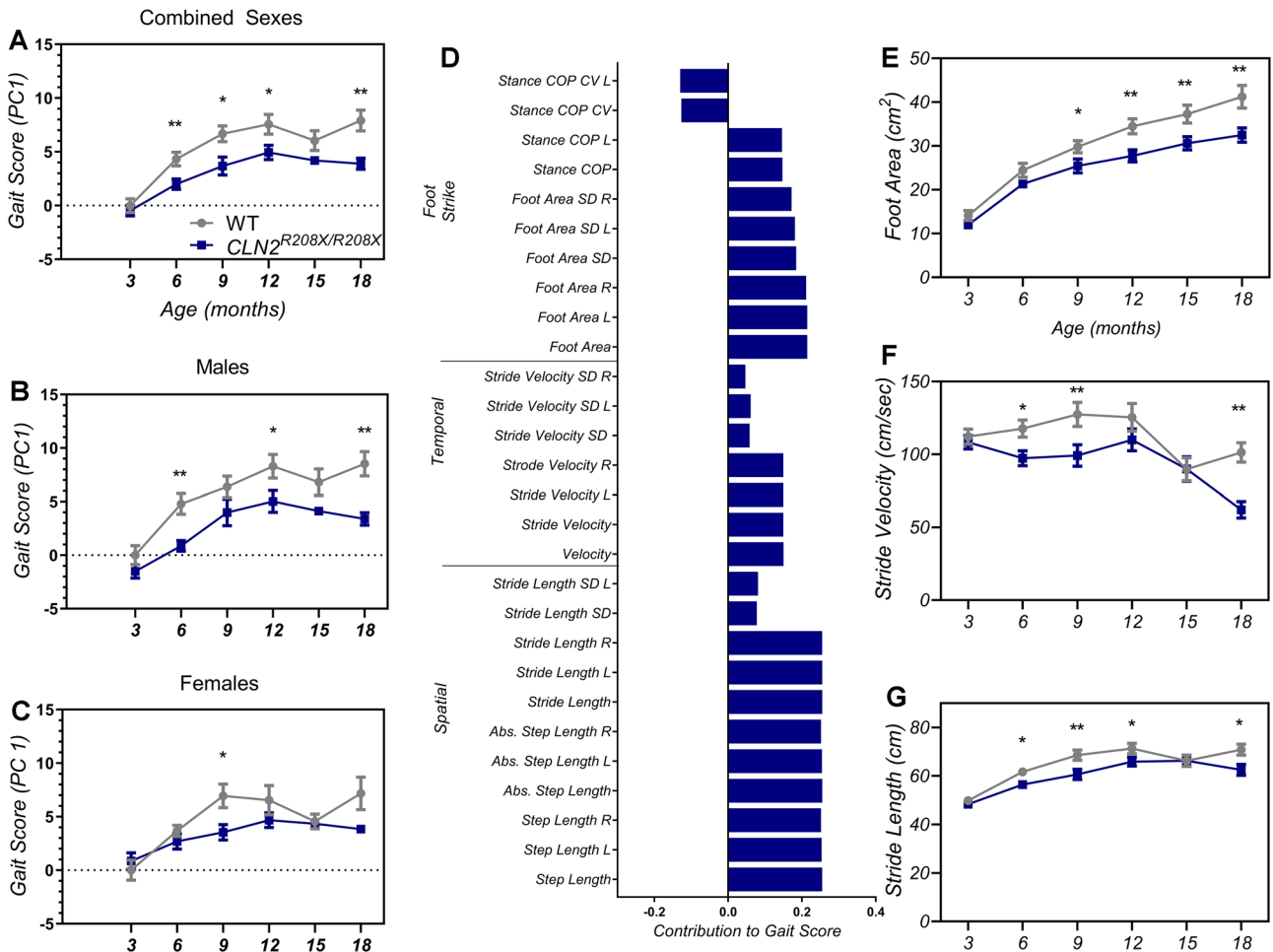
Fig. 3 $CLN2^{R208X/R208X}$ animals show consistent front foot gait abnormalities by 6 months of age. Principal component 1 (PC1) score for **A** combined sexes, **B** males, and **C** females, showing differences in gait between the genotypes. **D** Walkway parameters that contributed to front foot gait differences. **E** $CLN2^{R208X/R208X}$ animals place less of their foot on the walkway than wild-type animals. **F** $CLN2^{R208X/R208X}$ animals have a slower gait than wild-type animals. **G** $CLN2^{R208X/R208X}$ animals have shorter stride length than wild-type animals. Animal numbers in Supplemental Table 1. Mean ± SEM, Mixed-model ANOVA with uncorrected Fisher's LSD. $*p < 0.05$, $**p < 0.01$

$CLN2^{R208X/R208X}$ Miniswine Show Visual ERG Impairment by 6 to 9 Months of Age

Animals were assessed for visual deficits every three months from 3 to 18 months of age using an electroretinogram (ERG). $CLN2^{R208X/R208X}$ animals exhibit deficits in light-adapted cone responses (photopic tests, a- and b-waves) beginning at 6 months of age and continuing to 18 months of age (Fig. 4A), indicating deficits in both photoreceptors (a wave) and bipolar cells (b wave). Photopic scans indicate progressive declines of these waveforms as the $CLN2^{R208X/R208X}$ animals aged until all photopic waveforms were completely extinguished by 18 months, as indicated by slopes that are significantly different from zero. Deficits in dark-adapted rod responses (scotopic tests, a- and b-waves) began at 9 months of age and continued to 18 months of age (Fig. 4B). In $CLN2^{R208X/R208X}$ females, photopic deficits

arose at 12 months of age and scotopic at 12–15 months, with all waveforms declining through 18 months of age until completely extinguished (Fig. 4C, D). All waveform deficits arose earlier in $CLN2^{R208X/R208X}$ males, beginning at 9 months of age in both photopic and scotopic tests until all waveforms were completely extinguished by 18 months of age (Fig. 4E, F). Of note, the a- and b-waves declined after 9 months of age within both photopic and scotopic in the wild-type miniswine, possibly due to age related changes in the retina.

$CLN2^{R208X/R208X}$ Miniswine Lose Brain Volume and Have MRI Changes Similar to Patients with CLN2

The in vivo brain structure of $CLN2^{R208X/R208X}$ and wild-type animals was examined at 12 and 17 months of age via magnetic resonance imaging (MRI), showing evident changes in
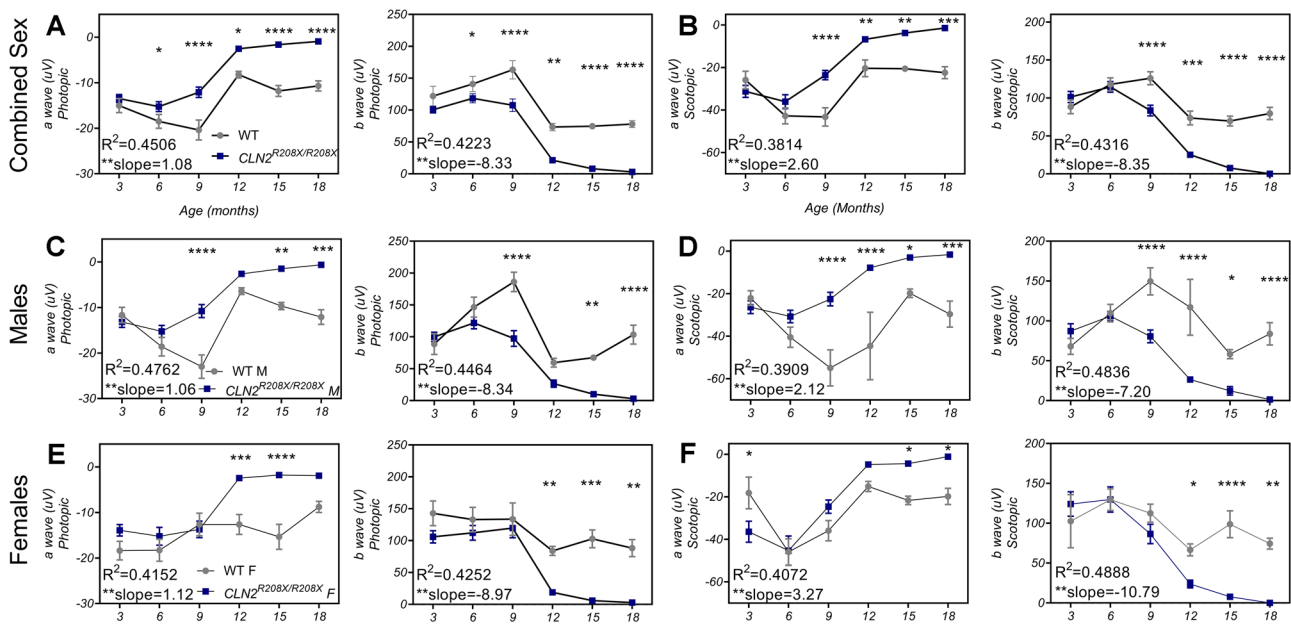
Fig. 4 $CLN2^{R208X/R208X}$ animals show electroretinogram (ERG) deficits by 6–9 months of age. ERG results from combined sexes for both **A** photopic and **B** scotopic protocols. ERG results from **C, D** male and **E, F** female animals, indicating that male $CLN2^{R208X/R208X}$ animals show ERG deficits slightly earlier than female animals. Animal numbers in Supplemental Table 1. Mean ± SEM, Two-way ANOVA with uncorrected Fisher's LSD. $*p < 0.05$, $**p < 0.01$, $***p < 0.001$, $****p < 0.0001$

caudate and ventricle structures as the disease progressed in $CLN2^{R208X/R208X}$ animals, compared to normal aging in wild-types (Fig. 5A). Segmentation of the intracranial volume (ICV) from MR indicated reduced ICV volume at both 12 and 17 months in $CLN2^{R208X/R208X}$ compared to wild-type (Fig. 5B). Cerebellar atrophy was qualitatively seen in the data; however, this was not quantitatively defined as more research is needed to develop a robust MRI atlas on the Yucatan miniswine brain.

Gross brain weight of 12- and 17-month-old wild-type and $CLN2^{R208X/R208X}$ miniswine was measured post-mortem. $CLN2^{R208X/R208X}$ animals showed brain atrophy at 12 and 17 months, as indicated by a decrease in brain weight (Fig. 5C). There was a linear relationship between the ICV measured in vivo and post-mortem gross brain weight (Fig. 5D). A sex-split analysis could be performed at 18 months of age as multiple male and female $CLN2^{R208X/R208X}$ animals had succumbed to the disease, which indicated that brain atrophy was similar between $CLN2^{R208X/R208X}$ animals of both sexes (Supplemental Fig. 5). Detailed MRI analysis of brain morphology in a sub-cohort of female miniswine is ongoing [37].

CLN2^{R208X/R208X} Animals Show Classic Batten Disease Pathology in Multiple Brain Regions

To determine if $CLN2^{R208X/R208X}$ animals show pathological hallmarks of CLN2 disease, brains were histologically examined for classic Batten disease pathology in several brain regions of both male and female animals at 6, 12, and 18 months of age (mixed sexes at each time point). These are common regions studied in CLN2 Batten disease models [7, 8, 13] as the VPM-VPL of the thalamus is one of the first brain regions to show classic Batten disease pathology [38], eventually affecting the thalamic relay inputs to the somatosensory cortex; and the motor cortex is involved in the coordination of movements, all neurocognitive functions that are impacted in Batten disease patients. In other animal models of CLN2, autofluorescent lipopigments have been examined in various brain regions as an indicator of storage material accumulation [7, 11, 39–43]. However, consistent and reproducible results have been shown with antibodies to mitochondrial ATP synthase subunit c (SubC) which labels storage material in the lysosomes of mice and dog models of CLN2 Batten disease [6, 8, 13, 44]. Compared to age matched, wild-type counterparts, SubC significantly accumulates in the somatosensory cortex (Fig. 6A, B), motor cortex (Fig. 6C, D), and ventral posteromedial/ventral posterolateral nuclei (VPM-VPL) of the thalamus (Fig. 6E, F) of $CLN2^{R208X/R208X}$ animals by 6 months of age, which is sustained until 18 months of age. Although not quantified, SubC also accumulated in other predominant gray matter regions such as the caudate, putamen, and dentate gyrus of the hippocampus.
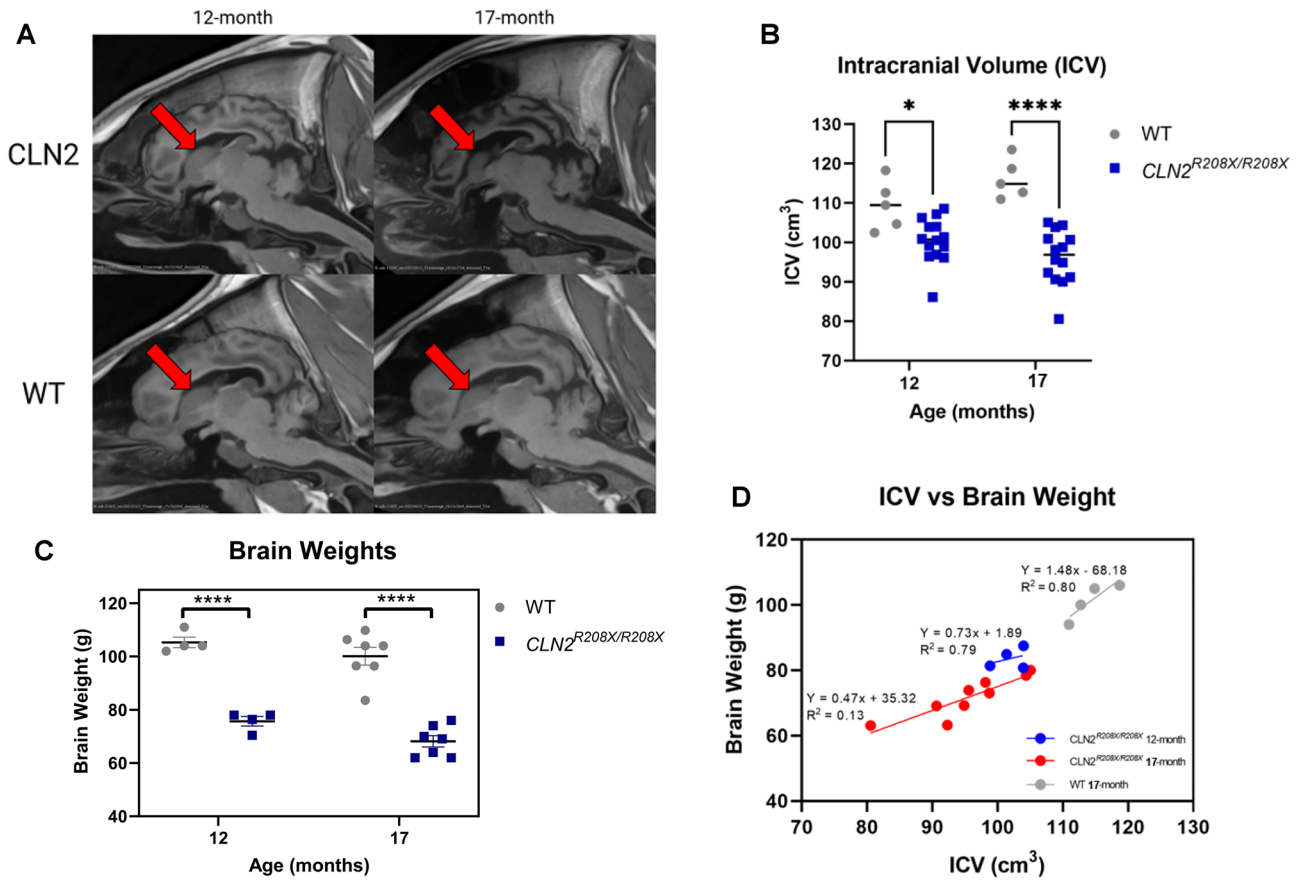
Fig. 5 $CLN2^{R208X/R208X}$ animals show MRI neurodegeneration that is similar to patients with CLN2 Batten disease. **A** Comparison of longitudinal $CLN2^{R20X/R208X}$ and WT T1-weighted MRI in aligned sagittal view, focusing on the caudate-ventricular border (red arrow), illustrates drastic longitudinal caudate shrinkage and ventricle enlargement of the CLN2 subject, compared to little noticeable longitudinal change in the WT subject. **B** Intracranial Volume (ICV) measured through segmentation of aligned MR data, illustrates significantly reduced ICV in $CLN2^{R20X/R208X}$ compared to wild-type animals. **C** $CLN2^{R208X/R208X}$ animals have lower brain mass than wild-type animals at 12 and 17 months of age. **D** Linear regression between in vivo measured ICV and post-mortem measured brain weight indicate it is possible to non-invasively approximate brain weight based on cohort type and age using MR. Animal numbers in Supplemental Table 1. Mean ± SEM, Two-way ANOVA or mixed-model ANOVA with uncorrected Fisher's LSD. $*p < 0.05$, $**p < 0.01$, $****p < 0.0001$

As neurodegeneration in Batten disease is commonly associated with neuroinflammatory cascades and glial activation, we labeled astrocytes with anti-GFAP antibodies and microglia with anti-IBA1 antibodies. We were unable to identify GFAP + astrocytes in the somatosensory cortex of 6- or 12-month animals. However, at 18 months, GFAP + astrocytes were evident in one of four $CLN2^{R208X/R208X}$ animals (Fig. 7A, B). Similarly in the motor cortex, GFAP + astrocytes were not observed in 6-month animals, but mild GFAP + astrocytosis was detected in one $CLN2^{R208X/R208X}$ animal at 12 and 18 months (Fig. 7C, D). Results for GFAP immunoreactivity did not reach statistical significance in either region at any time point. Lastly, in the VPM-VPL of the thalamus, there was no statistical difference at 6 months, but significant astrocytosis was identified in $CLN2^{R208X/R208X}$

animals at 12 and 18 months (Fig. 7E, F). Interestingly, prominent GFAP + labeling was found in the white matter tracts of the cerebral cortex, possibly indicating fibrous astrocytes.

To quantify microgliosis, microglia were labeled with anti-IBA1 antibodies, and the soma sizes were quantified to determine if microglia were changing to a more reactive, amoeboid shape [45]. We found more reactive microglia at 6, 12, and 18 months in the somatosensory cortex (Fig. 7G, H) and motor cortex (Fig. 7I, J) of $CLN2^{R208X/R208X}$ animals, with a particularly severe phenotype at 18 months of age. We did not see enlarged, reactive microglia at 6 or 12 months in the VPM-VPL of the thalamus. At 18 months, a few reactive microglia were found in the thalamus, but soma sizes were not significantly different between the two genotypes (Fig. 7K, L).
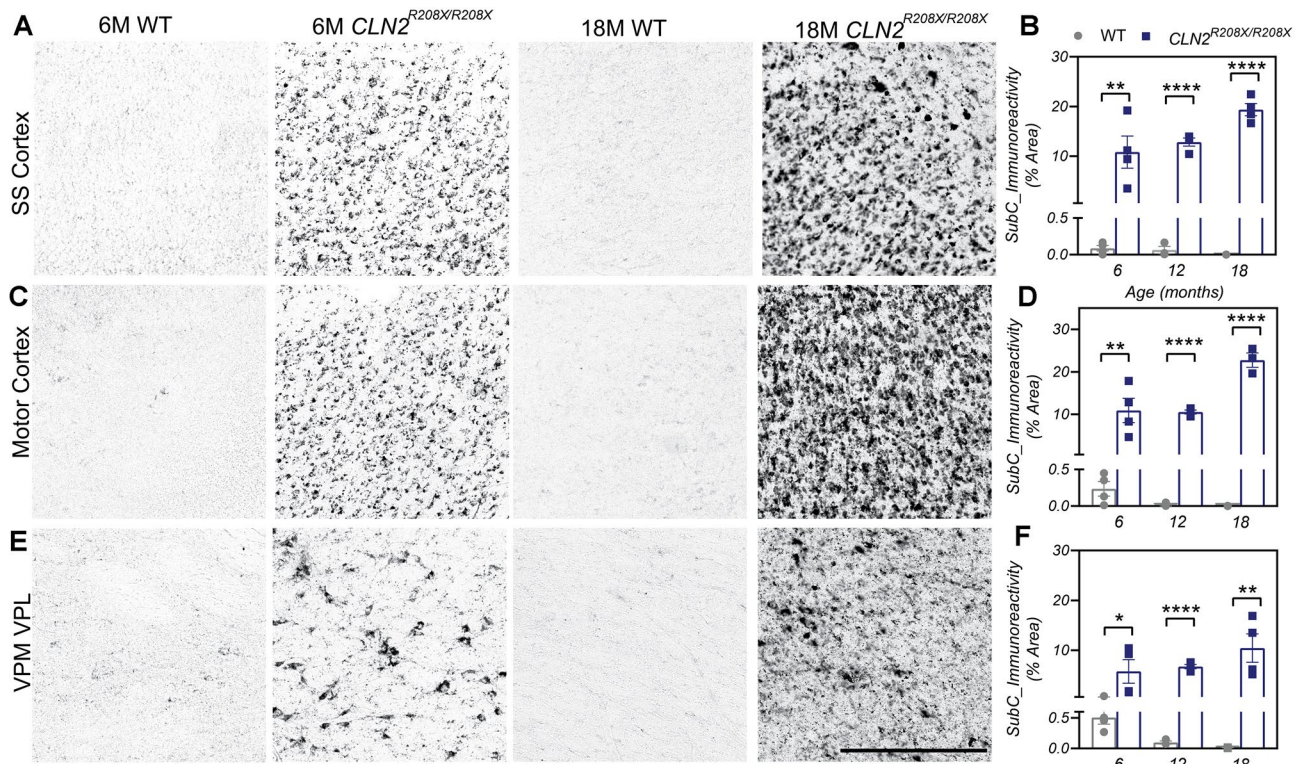
Fig. 6 Mitochondrial ATP synthase subunit c accumulates in the brains of *CLN2^{R208X/R208X}* animals. Subunit c accumulation shown in the **A**, **B** somatosensory cortex, **C**, **D** motor cortex, and **E**, **F** VPM/VPL of the thalamus, as early as 6 months of age. Animal numbers in Supplemental Table 1. Mean ± SEM, Nested *t* test at each time point, as histology was performed independently for each time point. *$p < 0.05$, **$p < 0.01$, ******$p < 0.0001$. Scale bar = 200 μm

Lastly, neurodegeneration as manifested by cortical thinning was examined. In *Cln2^{−/−}* mice, cortical atrophy of the neocortex (including the somatosensory regions) occurs at approximately 4.3 months of age [7]. The *CLN2^{R208X/R208X}* miniswine exhibited a decrease in the thickness of the cortical plate of the motor cortex at 6, 12, and 18 months, but this decrease was not significant ($p = 0.059$ at 18 months) (Fig. 8A). Cortical thinning of the somatosensory cortex of *CLN2^{R208X/R208X}* animals was significant at 18 months of age ($p = 0.003$, Fig. 8B). As the somatosensory and motor cortex were both affected in *CLN2^{R208X/R208X}* animals at 18 months of age, we further investigated if cell loss was isolated to specific cortical layers in these end-stage animals. NeuN+ cells were separated into eight equal sized bins across the cortical plate of the motor and somatosensory cortex to determine where cell loss was occurring. *CLN2^{R208X/R208X}* animals had significant cell loss in inner/deeper cortical layers (bin 7, Fig. 8C). When we examined subclasses of interneurons using immunohistochemistry, this cell loss was attributed in part to decreases in Calbindin + interneurons, while no difference was detected with Parvalbumin + neurons (Fig. 8D, E).

Discussion

Development of next-generation therapies for CLN2 disease has been hindered by a lack of robust large animal models with human-relevant pathogenic variants. Here, we present that *CLN2^{R208X/R208X}* miniswine recapitulate key presentations of CLN2 Batten disease. In comparison to the human condition, *CLN2^{R208X/R208X}* miniswine follow a similar disease course. *CLN2^{R208X/R208X}* gait and ERG abnormalities arise by approximately 6 months of age (3% of a typical 15-year lifespan) corresponding well to the onset of these presentations in CLN2 patients (3–5 years of age; 4–6% of a typical 73-year lifespan) [46, 47], and *CLN2^{R208X/R208X}* premature death at 18 months of age (10% of a typical lifespan) is consistent with patient premature death from 6 to 13 years of age (8 to 18% of a typical lifespan) [3, 48].

Our miniswine are declining rapidly after first onset of Batten disease phenotypes (within 3 months), with females (on average) succumbing to the disease about a month earlier than males. This rapid decline, indicating an earlier loss of independence and a more severe disease
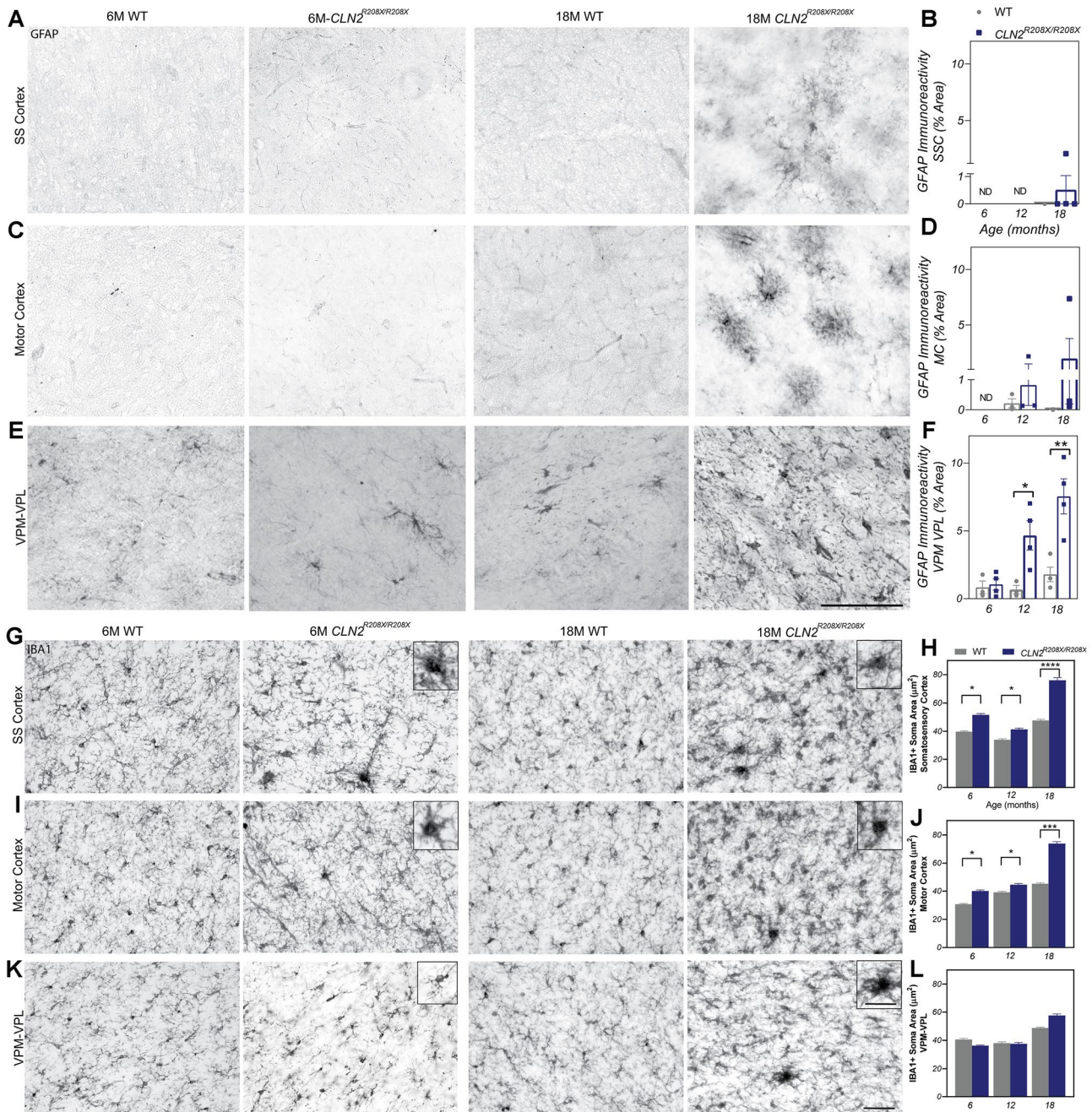
Fig. 7 $CLN2^{R208X/R208X}$ animals exhibit brain glial activation by 6–12 months of age. GFAP+astrocyte activation in the **A**, **B** somatosensory cortex, **C**, **D** motor cortex, and **E**, **F** VPM/VPL of the thalamus, as early as 12 months of age and most prominently in the thalamus. Iba1+microglial activation in the **G**, **H** somatosensory cortex, **I**, **J** motor cortex, and **K**, **L** VPM/VPL of the thalamus, as early as 6 months of age and as indicated by an increase in Iba1+soma size. Animal numbers in Supplemental Table 1. **A–F** Mean±SEM, unpaired t-test at each time point, as time points were run independently. $*p < 0.05$, $**p < 0.01$, $******p < 0.0001$. Scale bars=200 μm. **G–L** Mean±SEM, Nested t test at each time point, as histology was performed independently for each time point. $*p < 0.05$, $**p < 0.01$, $******p < 0.0001$. Scale bars=50 μm

course, has been previously described in female patients with other forms of Batten disease (i.e., CLN3 disease) and other NCL animal models [35, 49]. Though it appears that $CLN2^{R208X/R208X}$ females present with vision loss and balance declines before males, this earlier age of onset is not significantly different to the age of onset in the male counterparts. However, gait abnormalities and ERG deficits arise significantly sooner in $CLN2^{R208X/R208X}$ males than females, similar to the earlier onset of the disease in male patients with CLN3 [35].
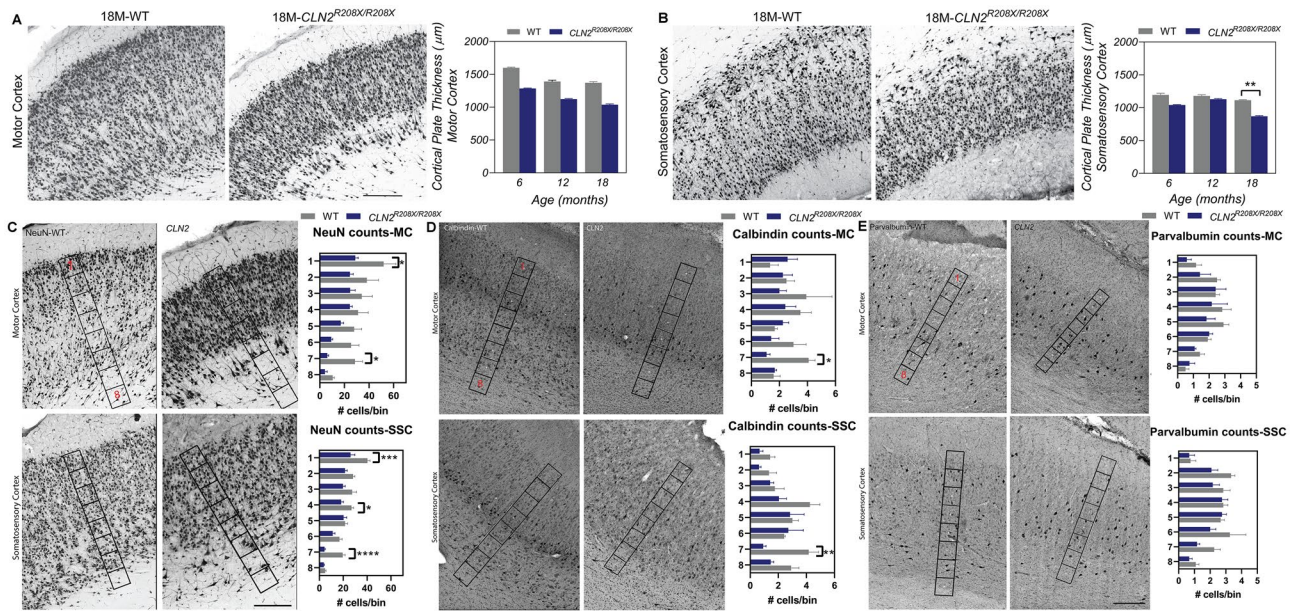
Fig. 8 $CLN2^{R208X/R208X}$ animals exhibit cortical thinning and loss of Calbindin + cortical neurons. Cortical plate thickness measurements in the **A** motor cortex and **B** somatosensory cortex, showing loss of overall cortical volume in $CLN2^{R208X/R208X}$ animals. **C** NeuN + neuronal counts in equally spaced cortical bins within the cortical plate in two cortical brain regions, showing loss of cells in the deeper layers of the cortex at 18 months of age. **D** Calbindin + neuronal counts show loss of calbindin + neurons in the deeper layers of the cortex at 18 months of age. **E** Parvalbumin + neuronal counts show no changes in two cortical brain regions at 18 months of age. Animal numbers in Supplemental Table 1. **A**, **B** Mean ± SEM, Nested t test at each time point, as histology was performed independently for each time point. $*p < 0.05$, $**p < 0.01$. Scale bar = 500 μm. **C–E** Mean ± SEM, two-way ANOVA with Sidak's multiple comparison test. $*p < 0.05$, $**p < 0.01$. Scale bar = 500 μm

Additionally, a- and b-wave declines are not completely reflective of vision loss. The amplitude of both a- and b-waves reduced after 9 months of age in the wild-type miniswine due to normal aging of the retina, and no overt vision loss was recorded in these animals. In other studies that utilized ERG data, wild-type miniswine did show a decline in scotopic b-wave amplitudes after 3 months of age and a slight decline in photopic b-wave amplitudes after 9 months of age [50]. In humans, scotopic and photopic b-waves reach maturity at 3–5 years of age [51]; and with normal aging of the retina, the decline of scotopic and photopic b-waves are highly correlated with age [52]. Similarly, ERG waveforms of the wildtype miniswine (especially the males) reach peak amplitude at 9 months of age (indicating maturity) and then begin to decline, with a greater magnitude of decline in the photopic and scotopic b-waves.

Though there may not be complete vision loss in the $CLN2^{R208X/R208X}$ miniswine, deteriorating vision and motor coordination that occurred (on average) around 15–17 months of age may have affected the performance of these animals in the simple t-maze at the 18-month testing. The animals had 60 s to complete each acquisition phase and another 60 s to complete each reversal phase, and the majority of the animals chose a response within that time. Two of the male $CLN2^{R208X/R208X}$ miniswine (out of eight tested)

failed to make choices during the 18-month testing. One of these male animals had developed earlier than average vision loss at 14 months of age, so may have been completely blind by the 18-month testing. Interestingly, two of the wild-type males (out of seven tested) failed to make choices at the 18-month testing as well. One of these wild-type males also failed to make t-maze choices at 12- and 15-months of age, indicating unwillingness of this animal to perform the test consistently. Besides these four animals, all others performed the t-maze at the 18-month time point within the allotted time; unlike t-maze testing in the $TPP1^{-/-}$ canine models, which was discontinued before end-stage either due to the refusal of the animals to complete the test or due to the inability of the animals to run the test due to severe motor and visual decline [10, 13]. Comparatively, CLN5 sheep were able to navigate the t-maze, though with longer travel times, as their vision was deteriorating [15]. To improve the t-maze testing, future tests will take into account the time to make a choice to investigate if the animals were losing the visual ability to navigate the maze.

Compared to other animal models of CLN2 disease, $CLN2^{R208X/R208X}$ miniswine more closely recapitulate the visual and seizure presentations of CLN2 patients. Specifically, $CLN2^{R208X/R208X}$ miniswine show an early photopic a-wave decline that resembles the loss of cone ERGs observed in

classic CLN2 patients, indicating a sensitivity of retinal cones to the loss of TPP1 [47]. $CLN2^{R208X/R208X}$ miniswine also show scotopic a- and b-wave declines by 9 months of age, which is similar to subnormal rod responses observed in 2-year-old patients with CLN2 [47, 53]. In contrast, while $TPP1^{-/-}$ canine models show ERG scotopic a-waves and photopic b-waves declining at similar ages to the $CLN2^{R208X/R208X}$ miniswine, the canine model shows inconsistent photopic a-wave declines, indicating species differences in retinal cone sensitivity to TPP1 loss [9, 10, 42, 54, 55]. These differences may be explained by the rod and cone distribution in each species' retinas as the rod to cone density of 3:1 in the central retina (within the visual streak) of the swine more closely matches the rod: cone density of 2:1 in human central retina (defined as 3° temporal retina and 3° nasal retina from optic nerve) [56, 57], unlike that seen in dogs with a much higher rod density of 22:1 in the central retina (area centralis) [58]. Lastly, tonic seizures have been observed in our $CLN2^{R208X/R208X}$ miniswine, whereas only tremors [6, 10, 13, 54], myoclonic bursts [7], and EEG abnormalities [12] are recorded in mice and dog models of CLN2. Though seizures have not been documented in $TPP1^{-/-}$ dogs, elevated creatine kinase, an indicator of seizure activity, has been reported in end stage animals [11]. Similarly, we see elevated creatine kinase in at least five out of eight $CLN2^{R208X/R208X}$ miniswine at 18 months of age compared to only one wild-type.

Children with CLN2 exhibit an ataxic, tumbling gait [46] with short steps beginning around 4 years of age [59], which is akin to the short-stepped, slow gait that was observed in $CLN2^{R208X/R208X}$ miniswine. Other animal studies have found motor and coordination deficits in both $Cln2^{-/-}$ mice (10–14 weeks of age) [6, 7, 41] and $TPP1^{-/-}$ dogs (7 months), where canines showed a wide-based stance [42] and an hypermetric [12] and ataxic gait [10]. Other large animal studies of Batten disease also confirm motor and coordination deficits (including hindlimb ataxia) [15]. Importantly, only one other study has completed a specific gait analysis that analyzed commonly known gait parameters, and showed that late-stage, 18-week-old $Cln2^{-/-}$ mice dragged their feet (increased hind limb stance and swing ratio) [40] and displayed asymmetry between front and hind feet [41]. Comparatively, we investigated 146 gait parameters that explained $CLN2^{R208X/R208X}$ gait based on foot strike, spatial, temporal, and balance characteristics, which allowed us to show male specific gait deficits early in disease course. This behavioral manifestation of disease has the potential to be a highly sensitive and translational biomarker for functional recovery from candidate therapies.

$CLN2^{R208X/R208X}$ miniswine also showed classic Batten disease histopathology (SubC accumulation, glial activation, and neuron loss), as seen in $Cln2^{-/-}$ mice [7, 41], $Cln2^{R207X/R207X}$ mice [6], and $TPP1^{-/-}$ dogs [12, 13, 42],

though astrocyte reactivity was notably mild and delayed in the cortical gray matter. Interestingly, another study in a miniswine model of Huntington's disease also showed a lack of reactive GFAP+ astrocytes in the cortex, indicating disparate reactivity of GFAP+ astrocytes in the cortical gray matter versus white matter in miniswine [24], similar to our findings. The differences in astrocyte reactivity may affect translational utility of the miniswine model in regard to testing astrocyte interacting compounds or better understanding the loss of TPP1 function in astrocytes. In the $CLN2^{R208X/R208X}$ miniswine, we see glial reactivity at 6 months, before cortical neuron loss at 18 months, which does resemble early glial activation in CLN2 patients [60] and mice. Loss of deeper layer cortical neurons and loss of cortical calbindin + and parvalbumin + interneurons have been identified in CLN2 patients [61], corresponding well to loss of cortical interneurons and reduction of intracranial volume in the $CLN2^{R208X/R208X}$ miniswine. MR imaging from other large animal models of Batten disease have previously shown a similar overall reduction in brain volumes and enlarged ventricles [14, 15], indicating the utility of this method to obtain reliable non-invasive imaging data as a biomarker on the progression of Batten disease.

In summary, $CLN2^{R208X/R208X}$ miniswine robustly recapitulate cognitive, visual, motor/gait, seizure, and premature death presentations as seen in CLN2 patients. $CLN2^{R208X/R208X}$ miniswine have enormous potential for investigations into the biology of CLN2 disease, biomarker discovery, and preclinical testing of therapies for patients with CLN2.

Methods

Animal Numbers

The number of animals examined for monthly in-pen monitoring, t-maze, gait assessment, ERGs, Fitbark, and immunohistochemistry are listed in Supplemental Table 1. Power analyses were not performed but animal numbers were predicted based on similar animal models of Batten disease [49, 62, 63].

Animal Phenotyping

Animals were monitored daily by Precigen Exemplar for general health and well-being and recorded monthly for specific Batten disease presentations. Visual capabilities were assessed by animal handlers noting if animals ran into walls or if animals could not track a hand moving in front of their eyes. Walking capabilities were assessed by animal handlers noting if animals were walking abnormally, if their limbs were weak, and/or if the animal was walking in

circles. Animal handlers also noted if any social or feeding behavior was abnormal, as well as whether a spontaneous seizure occurred.

Clinical Chemistries

Prior to euthanasia and after the animal was anesthetized with xylazine (TKX) and isoflurane, a 16 g needle was inserted into the right ventricle of the heart. The full syringe was emptied into a 10 mL blood collection tube via a Saf-T Holder™ transfer device, gently mixed by inversion and allowed to sit for 30 min. Collection tubes were centrifuged for $3100 \times g$ for 10 min at room temperature, and the resulting serum was either stored at -80 °C or sent to IDEXX BioAnalytics (North Grafton, MA) for clinical chemistry profile testing that included aspartate aminotransferase (AST) and creatine kinase (CK). The reference range for swine for AST is 14–61 U/L and for CK is 129–1409 U/L as reported by IDEXX.

Simple T-Maze

A simple t-maze was performed as previously described [22]. Briefly, animals were trained in a T-shaped apparatus using a food reward. For the acquisition phase, animals were given 60 s to find the arm that contained the food reward and were monitored over 10 trials each day for 2 days. For the reversal phase, the food reward was moved to the opposite arm and animals were again monitored for 10 trials each day for 2 days. The apparatus was thoroughly cleaned between each trial to reduce olfactory cues, and the initial position of the food reward was randomized between animals. The number of correct responses was monitored by a blinded observer that reviewed video footage of each trial (AnyMaze software v4.99; Stoelting Co. Wood Dale, IL). Animals that did not obtain 80% accuracy in the acquisition phase did not have their data analyzed for the reversal phase.

Gait Assessment

Animals were assessed for gait abnormalities using a Zeno walkway (ZenoMetrics Peekskill, NY) and PKMAS software (Protokinetics LLC, Havertown, PA) as previously described [23]. Briefly, animals were trained to walk along the walkway several times until five complete walks were obtained. Data was extracted and 153 variables were processed from the front feet and hind feet independently and analyzed using a principal component analysis (PCA) as previously described [64, 65] using the FactorMineR package in R.

Electroretinogram

Visual capabilities were assessed using a flash electroretinogram (ERG) RETeval device (LKC Technologies). Briefly, animals were anesthetized with 14 mg/kg ketamine (intramuscular) with anesthesia maintained with 1–2% isoflurane, and eyes dilated with 1% Tropicamide, Ophthalmic Solution, and anesthetized with 0.5% Proparacaine Hydrochloride–Ophthalmic Solution. Reference electrodes were connected to each ear and a ground electrode to the midline forehead via Ten20® conductive paste and flexible tape, and speculums were placed inside each eye to fix the eyelids open. DTL Plus Electrodes (LKC technologies) were attached to the rostral and caudal sides of each eye, and GenTeal® Tears, Lubricant Eye Gel was used to maintain electrode contact with each eye. The rabbit/minipig, photopic 2 step light adapted protocol (RETeval LKC Technologies) was used for photopic testing and produced an 8.0 cd s/m^2 flash @ 2 Hz flash followed by an 8.0 cd s/m^2 flicker @ 28.3 Hz (Supplemental Table 2). After photopic testing of both eyes, a heavy cloth was placed over the animal's head, all lights in the room were extinguished, and the animal allowed to dark adapt for 20 min. After dark adaption, the rabbit/minipig, scotopic 4 step protocol was used, which produced a 0.06 cd s/m^2 flash @ 0.5 Hz (dark adapted rod response), followed by an 8.0 cd s/m^2 flash @ 0.1 Hz (dark adapted mixed rod/cone response), followed by a 25 cd s/m^2 flash @ 0.05 Hz (dark adapted mixed rod/cone response to higher intensity flash) (Supplemental Table 2). Raw data values were used to calculate a-wave and b-wave amplitudes.

Fitbark Activity

General activity and sleep quality was monitored using a FitBark2 activity monitor as previously described [36]. Animals were monitored over 6 days using the activity monitor attached to their necks via a common dog or calf collar.

Magnetic Resonance Imaging

All neuroimaging procedures were performed as described in Knoernschild et al. [37]. Animals were anesthetized, intubated, and MR data acquired using a 3 T SIGNA Premier MRI scanner (GE Healthcare) with a medium 16-channel flexible coil (GE Healthcare). T1-weighted images utilized the BRAVO pulse sequence (TR/TE/TI/flip angle: 7.6/3.3/450 ms/12°; voxel size: $0.7 \times 0.7 \times 0.7$ mm^3) and T2-weighted images utilized the CUBE pulse sequence (TR/TE: 3000/51; voxel size: $0.7 \times 0.7 \times 0.7$ mm^3). To improve image quality and reduce potential motion artifacts, multiple shorter acquisitions were acquired and averaged (1–4

acquisitions, ~6 min each). T1- and T2-weighted images were processed, segmented, and analyzed according to Knoernschild et al. [37].

Immunohistochemistry

Both female and male animals were sacrificed with pentobarbital at 6, 12, and 18 months of age, and one hemisphere of the brain placed into 10% neutral-buffered formalin for approximately 3 weeks. The brain was subsequently subdissected into region-specific blocks, which were equilibrated in cryoprotectant solution (30% sucrose in TBSA) at 4 °C. Blocks were serial sectioned (50 µm) on a freezing microtome (Leica) and free-floating sections from the somatosensory cortex, motor cortex, and VPM-VPL of the thalamus were used for standard immunohistochemistry [49, 63, 66–68]. The following primary antibodies were used: anti-mitochondrial ATP synthase subunit C (Abcam, ab181243; 1:2000), anti-GFAP (Dako, Z0334; 1:16,000), anti-IBA1 (BioCare Medical, 290; 1:2000), anti-NeuN (Millipore Sigma, MAB377; 1:2000), anti-Calbindin (Swant, CB38; 1:2000), and anti-Parvalbumin (Swant, PV27, 1:2500). Secondary antibodies were goat anti-rabbit or goat anti-mouse depending on the host of the primary antibody. Immunolabeled sections were scanned using an Aperio Versa slide scanner (Leica Biosystems, IL, USA) or Nikon 90i microscope (Nikon instruments, Inc, NY, USA), and at least 3 images were extracted from each region of interest, condensed by Adobe Photoshop, and split into RGB channels by ImageJ (NIH) [69]. Adjusted ImageJ threshold and analyze particles settings were used to measure total percent area of SubC and GFAP immunolabeling, and to measure soma size/number of IBA1, calbindin, and parvalbumin immunolabeling. For NeuN, cortical plate thickness was measured in coronal sections of the somatosensory and motor cortex following methods previously published [49].

Statistics

All data was analyzed in Graphpad Prism 9.0 or equivalent using the statistical tests described in the figure legends: $*p < 0.05$, $**p < 0.01$, $***p < 0.001$, $****p < 0.0001$.

Study Approval

All animals were maintained at Precigen Exemplar under an approved IACUC protocol (Protocol # MRP2018-004). All neuroimaging procedures were approved by the Institutional Animal Care and Use Committees (IACUC) of the University of Iowa and Precigen Exemplar in accordance with regulations and were performed as described in Knoernschild et al. [37].

Declarations

Conflict of Interest The authors declare no conflict of interest.

References

1. Wisniewski KE, Kida E, Golabek AA, Kaczmarski W, Connell F, Zhong N. Neuronal ceroid lipofuscinoses: classification and diagnosis. Adv Genet. 2001;45:1–34.
2. Shyng C, Nelvagal HR, Dearborn JT, et al. Synergistic effects of treating the spinal cord and brain in CLN1 disease. Proc Natl Acad Sci U S A. 2017;114(29):E5920–9.
3. Goebel HH, Wisniewski KE. Current state of clinical and morphological features in human NCL. Brain Pathol. 2004;14(1):61–9.
4. Gardner E, Mole SE. The genetic basis of phenotypic heterogeneity in the neuronal ceroid lipofuscinoses. Front Neurol. 2021;12:754045.
5. Kousi M, Lehesjoki AE, Mole SE. Update of the mutation spectrum and clinical correlations of over 360 mutations in eight genes that underlie the neuronal ceroid lipofuscinoses. Hum Mutat. 2012;33(1):42–63.
6. Geraets RD, Langin LM, Cain JT, et al. A tailored mouse model of CLN2 disease: a nonsense mutant for testing personalized therapies. PLoS ONE. 2017;12(5):e0176526.
7. Sleat DE, Wiseman JA, El-Banna M, et al. A mouse model of classical late-infantile neuronal ceroid lipofuscinosis based on targeted disruption of the CLN2 gene results in a loss of tripeptidyl-peptidase I activity and progressive neurodegeneration. J Neurosci. 2004;24(41):9117–26.
8. Takahashi K, Eultgen EM, Wang SH, et al. Cortical interneuron loss and seizure generation as novel clinically relevant disease phenotypes in $Cln2^{R207X}$ mice. bioRxiv. 2022. https://doi.org/10.1101/2022.03.11.483984.
9. Katz ML, Coates JR, Cooper JJ, O'Brien DP, Jeong M, Narfstrom K. Retinal pathology in a canine model of late infantile neuronal ceroid lipofuscinosis. Invest Ophthalmol Vis Sci. 2008;49(6):2686–95.
10. Katz ML, Coates JR, Sibigtroth CM, et al. Enzyme replacement therapy attenuates disease progression in a canine model of late-infantile neuronal ceroid lipofuscinosis (CLN2 disease). J Neurosci Res. 2014;92(11):1591–8.

11. Katz ML, Johnson GC, Leach SB, et al. Extraneuronal pathology in a canine model of CLN2 neuronal ceroid lipofuscinosis after intracerebroventricular gene therapy that delays neurological disease progression. Gene Ther. 2017;24(4):215–23.

12. Awano T, Katz ML, O'Brien DP, et al. A frame shift mutation in canine TPP1 (the ortholog of human CLN2) in a juvenile Dachshund with neuronal ceroid lipofuscinosis. Mol Genet Metab. 2006;89(3):254–60.

13. Katz ML, Tecedor L, Chen Y, et al. AAV gene transfer delays disease onset in a TPP1-deficient canine model of the late infantile form of Batten disease. Sci Transl Med. 2015;7(313):313ra180.

14. Eaton SL, Proudfoot C, Lillico SG, et al. CRISPR/Cas9 mediated generation of an ovine model for infantile neuronal ceroid lipofuscinosis (CLN1 disease). Sci Rep. 2019;9(1):9891.

15. Mitchell NL, Russell KN, Wellby MP, et al. Longitudinal in vivo monitoring of the CNS demonstrates the efficacy of gene therapy in a sheep model of CLN5 Batten disease. Mol Ther. 2018;26(10):2366–78.

16. Tammen I, Houweling PJ, Frugier T, et al. A missense mutation (c.184C>T) in ovine CLN6 causes neuronal ceroid lipofuscinosis in Merino sheep whereas affected South Hampshire sheep have reduced levels of CLN6 mRNA. Biochim Biophys Acta. 2006;1762(10):898–905.

17. Tammen I, Cook RW, Nicholas FW, Raadsma HW. Neuronal ceroid lipofuscinosis in Australian Merino sheep: a new animal model. Eur J Paediatr Neurol. 2001;5(Suppl A):37–41.

18. Palmer DN, Neverman NJ, Chen JZ, et al. Recent studies of ovine neuronal ceroid lipofuscinoses from BARN, the Batten Animal Research Network. Biochim Biophys Acta. 2015;1852(10 Pt B):2279–86.

19. Yang L, Church G, Zhao HY, et al. Porcine germline genome engineering. Proc Natl Acad Sci U S A. 2021;118(22).

20. Swindle MM, Makin A, Herron AJ, Clubb FJ Jr, Frazier KS. Swine as models in biomedical research and toxicology testing. Vet Pathol. 2012;49(2):344–56.

21. Nair AB, Jacob S. A simple practice guide for dose conversion between animals and human. J Basic Clin Pharm. 2016;7(2):27–31.

22. White KA, Swier VJ, Cain JT, et al. A porcine model of neurofibromatosis type 1 that mimics the human disease. JCI Insight. 2018;3(12).

23. Beraldi R, Chan CH, Rogers CS, et al. A novel porcine model of ataxia telangiectasia reproduces neurological features and motor deficits of human disease. Hum Mol Genet. 2015;24(22):6473–84.

24. Ardan T, Baxa M, Levinská B, et al. Transgenic minipig model of Huntington's disease exhibiting gradually progressing neurodegeneration. Dis Model Mech. 2019;13(2):dmm041319.

25. Kragh PM, Nielsen AL, Li J, et al. Hemizygous minipigs produced by random gene insertion and handmade cloning express the Alzheimer's disease-causing dominant mutation APPsw. Transgenic Res. 2009;18(4):545–58.

26. Fang M, Lorke DE, Li J, Gong X, Yew JC, Yew DT. Postnatal changes in functional activities of the pig's brain: a combined functional magnetic resonance imaging and immunohistochemical study. Neurosignals. 2005;14(5):222–33.

27. Villadsen J, Hansen HD, Jorgensen LM, et al. Automatic delineation of brain regions on MRI and PET images from the pig. J Neurosci Methods. 2018;294:51–8.

28. Uthoff J, Larson J, Sato TS, et al. Longitudinal phenotype development in a minipig model of neurofibromatosis type 1. Sci Rep. 2020;10(1):5046.

29. Sieren JC, Meyerholz DK, Wang XJ, et al. Development and translational imaging of a TP53 porcine tumorigenesis model. J Clin Invest. 2014;124(9):4052–66.

30. Hammond E, Newell JD Jr, Dilger SK, et al. Computed tomography and magnetic resonance imaging for longitudinal characterization of lung structure changes in a Yucatan miniature pig silicosis model. Toxicol Pathol. 2016;44(3):373–81.

31. van der Laan JW, Brightwell J, McAnulty P, Ratky J, Stark C, Steering Group of the RP. Regulatory acceptability of the minipig in the development of pharmaceuticals, chemicals and other products. J Pharmacol Toxicol Methods. 2010;62(3):184–95.

32. Brudvig JJ, Swier VJ, Johnson TB, et al. Glycerophosphoinositol is elevated in blood samples from CLN3Δex7–8 pigs, Cln3Δex7–8 mice, and human patients with CLN3 disease. in prep.

33. Rogers CS, Stoltz DA, Meyerholz DK, et al. Disruption of the CFTR gene produces a model of cystic fibrosis in newborn pigs. Science. 2008;321(5897):1837–41.

34. Nielsen AK, Ostergaard JR. Do females with juvenile ceroid lipofuscinosis (Batten disease) have a more severe disease course? The Danish experience. Eur J Paediatr Neurol. 2013;17(3):265–8.

35. Cialone J, Adams H, Augustine EF, et al. Females experience a more severe disease course in Batten disease. J Inherit Metab Dis. 2012;35(3):549–55.

36. Khanna R, Moutal A, White KA, et al. Assessment of nociception and related quality-of-life measures in a porcine model of neurofibromatosis type 1. Pain. 2019;160(11):2473–86.

37. Knoernschild K, Johnson H, Schroeder K, et al. Magnetic resonance brain volumetry biomarkers of Batten disease identified with minipig model in prep for submission to American Journal of Neuroradiology. 2022.

38. Kielar C, Maddox L, Bible E, et al. Successive neuron loss in the thalamus and cortex in a mouse model of infantile neuronal ceroid lipofuscinosis. Neurobiol Dis. 2007;25(1):150–62.

39. Katz ML, Rustad E, Robinson GO, et al. Canine neuronal ceroid lipofuscinoses: promising models for preclinical testing of therapeutic interventions. Neurobiol Dis. 2017;108:277–87.

40. Cabrera-Salazar MA, Roskelley EM, Bu J, et al. Timing of therapeutic intervention determines functional and survival outcomes in a mouse model of late infantile batten disease. Mol Ther. 2007;15(10):1782–8.

41. Sondhi D, Hackett NR, Peterson DA, et al. Enhanced survival of the LINCL mouse following CLN2 gene transfer using the rh.10 rhesus macaque-derived adeno-associated virus vector. Mol Ther. 2007;15(3):481–91.

42. Vuillemenot BR, Katz ML, Coates JR, et al. Intrathecal tripeptidyl-peptidase 1 reduces lysosomal storage in a canine model of late infantile neuronal ceroid lipofuscinosis. Mol Genet Metab. 2011;104(3):325–37.

43. Passini MA, Dodge JC, Bu J, et al. Intracranial delivery of CLN2 reduces brain pathology in a mouse model of classical late infantile neuronal ceroid lipofuscinosis. J Neurosci. 2006;26(5):1334–42.

44. Sleat DE, El-Banna M, Sohar I, et al. Residual levels of tripeptidyl-peptidase I activity dramatically ameliorate disease in late-infantile neuronal ceroid lipofuscinosis. Mol Genet Metab. 2008;94(2):222–33.

45. Davis BM, Salinas-Navarro M, Cordeiro MF, Moons L, De Groef L. Characterizing microglia activation: a spatial statistics approach to maximize information extraction. Sci Rep. 2017;7(1):1576.

46. Ostergaard JR. Gait phenotype in Batten disease: a marker of disease progression. Eur J Paediatr Neurol. 2021;35:1–7.

47. Thompson DA, Handley SE, Henderson RH, Marmoy OR, Gissen P. An ERG and OCT study of neuronal ceroid lipofuscinosis CLN2 Battens retinopathy. Eye (Lond). 2021;35(9):2438–48.

48. Gardner E, Bailey M, Schulz A, Aristorena M, Miller N, Mole SE. Mutation update: review of TPP1 gene variants associated with neuronal ceroid lipofuscinosis CLN2 disease. Hum Mutat. 2019;40(11):1924–38.

49. Poppens MJ, Cain JT, Johnson TB, et al. Tracking sex-dependent differences in a mouse model of CLN6-Batten disease. Orphanet J Rare Dis. 2019;14(1):19.

50. Scott PA, de Castro JP, DeMarco PJ, et al. Progression of Pro-23His retinopathy in a miniature swine model of retinitis pigmentosa. Transl Vis Sci Technol. 2017;6(2):4.

51. Westall CA, Panton CM, Levin AV. Time courses for maturation of electroretinogram responses from infancy to adulthood. Doc Ophthalmol. 1998;96(4):355–79.

52. Weleber RG. The effect of age on human cone and rod ganzfeld electroretinograms. Invest Ophthalmol Vis Sci. 1981;20(3):392–9.

53. Weleber RG. The dystrophic retina in multisystem disorders: the electroretinogram in neuronal ceroid lipofuscinoses. Eye (Lond). 1998;12(Pt 3b):580–90.

54. Sanders DN, Kanazono S, Wininger FA, et al. A reversal learning task detects cognitive deficits in a Dachshund model of late-infantile neuronal ceroid lipofuscinosis. Genes Brain Behav. 2011;10(7):798–804.

55. Whiting RE, Narfstrom K, Yao G, et al. Pupillary light reflex deficits in a canine model of late infantile neuronal ceroid lipofuscinosis. Exp Eye Res. 2013;116:402–10.

56. Wells-Gray EM, Choi SS, Bries A, Doble N. Variation in rod and cone density from the fovea to the mid-periphery in healthy human retinas using adaptive optics scanning laser ophthalmoscopy. Eye. 2016;30(8):1135–43.

57. Chandler MJ, Smith PJ, Samuelson DA, MacKay EO. Photoreceptor density of the domestic pig retina. Vet Ophthalmol. 1999;2(3):179–84.

58. Mowat FM, Petersen-Jones SM, Williamson H, et al. Topographical characterization of cone photoreceptors and the area centralis of the canine retina. Mol Vis. 2008;14:2518–27.

59. Di Giacopo R, Cianetti L, Caputo V, et al. Protracted late infantile ceroid lipofuscinosis due to TPP1 mutations: Clinical, molecular and biochemical characterization in three sibs. J Neurol Sci. 2015;356(1–2):65–71.

60. Tyynela J, Cooper JD, Khan MN, Shemilts SJ, Haltia M. Hippocampal pathology in the human neuronal ceroid-lipofuscinoses: distinct patterns of storage deposition, neurodegeneration and glial activation. Brain Pathol. 2004;14(4):349–57.

61. Hachiya Y, Hayashi M, Kumada S, Uchiyama A, Tsuchiya K, Kurata K. Mechanisms of neurodegeneration in neuronal ceroid-lipofuscinoses. Acta Neuropathol. 2006;111(2):168–77.

62. Cain JT, Likhite S, White KA, et al. Gene therapy corrects brain and behavioral pathologies in CLN6-Batten disease. Mol Ther. 2019.

63. Johnson TB, White KA, Brudvig JJ, et al. AAV9 Gene therapy increases lifespan and treats pathological and behavioral abnormalities in a mouse model of CLN8-batten disease. Mol Ther. 2021;29(1):162–75.

64. Johnson TB, Brudvig JJ, Lehtimaki KK, et al. A multimodal approach to identify clinically relevant biomarkers to comprehensively monitor disease progression in a mouse model of pediatric neurodegenerative disease. Prog Neurobiol. 2020;189:101789.

65. Le S, Josse J, Husson F. FactoMineR: an R package for multivariate analysis. J Stat Softw. 2008;25(1):1–18.

66. Swier VJ, White KA, Meyerholz DK, et al. Validating indicators of CNS disorders in a swine model of neurological disease. PLoS ONE. 2020;15(2):e0228222.

67. Langin L, Johnson TB, Kovacs AD, Pearce DA, Weimer JM. A tailored Cln 3(Q352X) mouse model for testing therapeutic interventions in CLN3 Batten disease. Sci Rep. 2020;10(1):10591.

68. Johnson TB, Langin LM, Zhao J, Weimer JM, Pearce DA, Kovacs AD. Changes in motor behavior, neuropathology, and gut microbiota of a Batten disease mouse model following administration of acidified drinking water. Sci Rep. 2019;9(1):14962.

69. Schneider CA, Rasband WS, Eliceiri KW. NIH Image to ImageJ: 25 years of image analysis. Nat Methods. 2012;9(7):671–5.